ARTICLE

Fabrication and SERS Performance of Silver-Nanoparticle-Decorated Si/ZnO Nanotrees in Ordered Arrays

Chuanwei Cheng,[†] Bin Yan,[†] She Mein Wong,[‡] Xianglin Li,[†] Weiwei Zhou,[†] Ting Yu,[†] Zexiang Shen,[†] Hongyu Yu,[‡] and Hong Jin Fan[†,*]

Division of Physics and Applied Physics, School of Physical and Mathematical Sciences, Nanyang Technological University, 637371 Singapore, and Division of Microelectronics, School of Electrical and Electronic Engineering, Nanyang Technological University, 639798 Singapore

ABSTRACT Highly ordered treelike Si/ZnO hierarchical nanostructures are successfully prepared in a large scale by combining two common techniques, viz., photolithography-assisted wafer-scale fabrication of Si nanopillars and bottom-up hydrothermal growth of ZnO nanorods. Silver nanoparticles are decorated onto the nanotrees by photochemical reduction and deposition. The Si/ZnO/Ag hybrid nanotrees are employed as SERS-active substrates, which exhibit good performance in terms of high sensitivity and good reproducibility. In addition to the SERS application, such ordered Si/ZnO arrays might also find potential applications in light-emitting diodes and solar cells.

KEYWORDS: Si nanowire • ZnO nanorod • hierarchical • hydrothermal, SERS

INTRODUCTION

Rational design and fabrication of hierarchical nanostructures with a tunable dimension and structural complexity have drawn wide attention because of their promising applications in nanoelectronic devices, energy conversion, SERS (surface-enhanced Raman spectroscopy) substrate, and so on (1−5). For example, various groups have reported treelike nanostructures of GaP (6), Zn_3P_2 (7), PbS (8), and TiO_2 (9). Recently we developed a facile method to fabricate tree-like hierarchical nanostructures with ZnO branches on SnO_2 backbone nanowires in a large scale by a two-step fabrication process (4).

Since its discovery 30 years ago (10−12), SERS as a powerful high-throughput tool for trace-level molecule detection has stimulated considerable research interest in the scientific community (13−18). In the past few years, much progress has been made in the fabrication of various metal nanostructures as Raman signal enhancing agents (19−23). Recently, it has been demonstrated that using three-dimensional (3D) nanostructures as SERS media can dramatically increase the sensitivity (24−30). The 3D nanostructures have advantages of large surface area available for the formation of the so-called "hot spots" (spatially localized surface plasmon resonances between those closely neighbored nanoparticles) (31) and the adsorption of target analytes. A number of promising 3D SERS substrates have been proposed, such as porous Si (24) and Al_2O_3 nanochanels (25), Si nanotips (26) and nanowires (27), ZnO nanowire arrays (28, 29), and In_2P_3 nanowire arrays (30).

To bring SERS-based sensor to practical applications, it is desirable that the SERS substrates contain of highly ordered structures with reproducible and controllable geometries. A nanopatterned structure, either 3D or 2D, can provide significant Raman enhancement. A number of techniques are available for 2D patterning of SERS substrates, ranging from the conventional electron beam lithography (32, 33) photolithography (34), to the mordern nanosphere lithography (35), block copolymer lithography (36, 37), etc. Among these approaches, photolithography has its advantage in terms of large area, high-throughput with relatively low cost, and most importantly, technical compatibility with Si industry, which is essential for realizing lab-on-a-chip sensing devices.

In this paper, we fabricated highly ordered treelike Si/ZnO hierarchical nanostructure arrays by combining photolithography top-down patterning toward ordered Si nanopillar arrays, and subsequent hydrothermal growth of ZnO nanorods on the Si pillars. The obtained ordered arrays of nanotrees are then coated with Ag nanoparticles in order for SERS applications. Compared to SERS substrates based on nanoparticles films (37) and unidirectional nanowire arrays (26−30), the nanotrees have a much higher specific surface area, thus allowing an increased loading of metal particles and adsorption of a larger number of target molecules, as well as the high possibility of forming 3D plasmon "hot spots". In addition, it is expected that such ordered patterns can be readily integrated within microfluidic channels and applied in high-throughput screening bioassays.

RESULTS AND DISCUSSION

Figure 1 illustrates the fabrication procedure for the 3D hierarchical SERS substrates. The process mainly involves

* Corresponding author. E-mail: fanhj@ntu.edu.sg.
Received for review March 27, 2010 and accepted May 21, 2010
[†] School of Physical and Mathematical Sciences, Nanyang Technological University.
[‡] School of Electrical and Electronic Engineering, Nanyang Technological University.
DOI: 10.1021/am100270b

Published on Web 06/01/2010

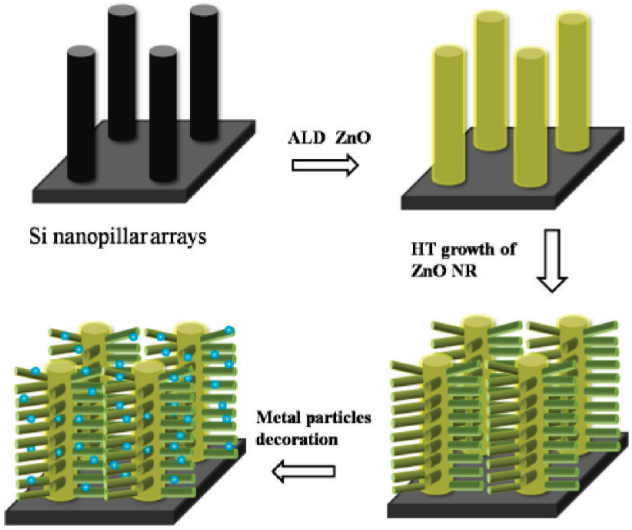

FIGURE 1. Schematics of the fabrication procedures for the 3D hierarchical SERS substrate, which is ordered Si/ZnO nanotrees decorated by silver nanoparticles.

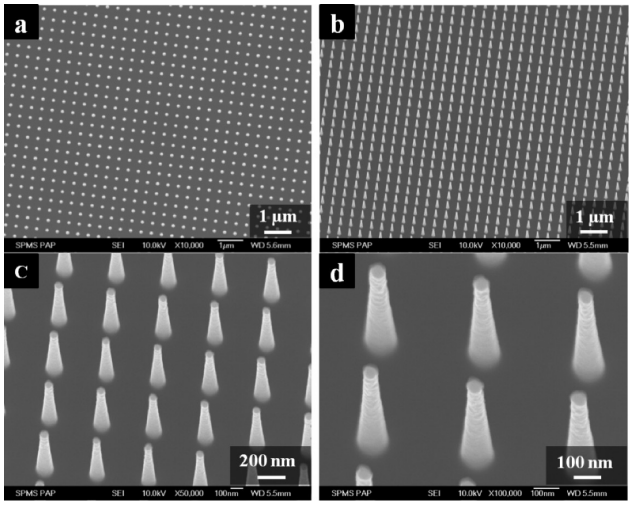

FIGURE 2. SEM images of the Si nanopillar arrays. (a) Top view and (b) 20° titled view.

three steps. First, the patterned Si nanopillar arrays were prepared by standard top-down photolithography followed by dry etching. This step defines the height and interdistance of the trunks. In order to ensure the structure robustness and preserve the patterns, the Si nanopillars herein are relatively thick and short (see below). Subsequently, ZnO branches were grown on the Si nanopillars through a routine hydrothermal process. The lengths of the nanorods are adustable by controlling the growth time (1−5 h). The ZnO seed layer needed for the hydrothermal growth was coated using atomic layer deposition, which is particularly advantageous in the case of high-aspect-ratio Si pillars. Finally, Ag nanoparticles were loaded onto the nanotrees through photochemical reduction and deposition.

Figure 2a−d show the top and tilted-view SEM images of the as-prepared Si nanopillar arrays on Si substrate after etching. The pillars are oriented perpendicular to the substrate surface with good uniformity. The pillar shows a towerlike morphology with a typical height of 300 nm, the average diameter of Si pillar is about 150 nm and gradually decreases from the root to the tip. The nearest-neighbor spacing of the pillars is 400 nm, as predefined by shadow mask.

After applying the solution growth of ZnO nanorods, the initially smooth Si pillars branch out, forming tree-like nanostructures. The typical SEM images of such structures are shown in Figure 3a−d. The ZnO nanorod branches are mainly stand perpendicular to the side surfaces of the Si pillars. From the magnified SEM images (Figure 3c,d), the diameter and length of secondary ZnO nanorods are determined to be about 30 nm and 150−200 nm, respectively. The length of ZnO nanorods are controllable by adjusting the growth time (see Figure S1 in the Supporting Information). Unlike the cases of SnO_2 nanowire backbones where the interface epitaxy allows a spacial alignment of the ZnO nanorods (4), the ZnO nanorod branches on the Si pillars are randomly oriented.

Figure 4 shows the representative SEM image of the ordered nanotrees whose branches are decorated with Ag nanoparticles. The metal Ag nanoparticles are successfully deposited onto the surface of both ZnO branches and Si backbones. The diameter of Ag particles is about 20−30 nm. The successful decoation can be more clearlier seen in samples with longer ZnO branches (see the Supporting Information. Figure S2). X-ray diffraction (XRD) analysis was employed to investigate the crystal phase of nanotrees prior to and after the Ag decoration (see the Supporting Information, Figure S3). The crystal phase of ZnO marked with"Δ" is confirmed to be hexagonal wurtzite phase, and the peaks marked with "♦" (curve b) can be indexed to face-centered-cubic (fcc) structure of Ag.

To evaluate the SERS activity of the Si/ZnO/Ag nanotree substrates, we measured Raman spectra of R6G molecules adsorbed on three types of different samples: bare Si/ZnO nanotrees, Si/ZnO/Ag nanotrees, and Ag particles on a flat Si surface. The results are depicted in Figure 5. Curve a is from the Si/ZnO nanotrees incubated in 10^{-5} M R6G solution for 20 min and then washed with deionized water (i.e., without Ag decoration). Only one strong Raman peak located at ∼520 cm^{-1} is observed, which is assigned to the first-order optical phonon scattering of crystal Si nanopillars and substrate. No R6G related Raman signals can be observed in curve a. For the Si/ZnO/Ag sample (curve c), besides the Si peak, very strong R6G characteristic peaks are present. The Raman bands at 1650, 1570, 1507, 1357, 1310, 1180, 778, and 605 cm^{-1} are assigned to the xanthene ring stretch, ethylamine group wag, and carbon−oxygenstretch of R6G (38). For comparison, a control Raman study on 2D Ag nanoparticles with diameter of ∼15 nm (see Figure S4 in the Supporting Information for SEM image) on planar Si substrate was conducted. As shown in curve b, the Raman enhancement is much weaker than that of the Si/ZnO/Ag nanotree structures. Furthermore, the SERS detection level of R6G molecules for the Si/ZnO/Ag substrates can reach to 1×10^{-9} M (see the Supporting Information, Figure S5).

Quantifying the absolute enhancement factor (EF) is still a matter of debate in literature, which requires accurate data

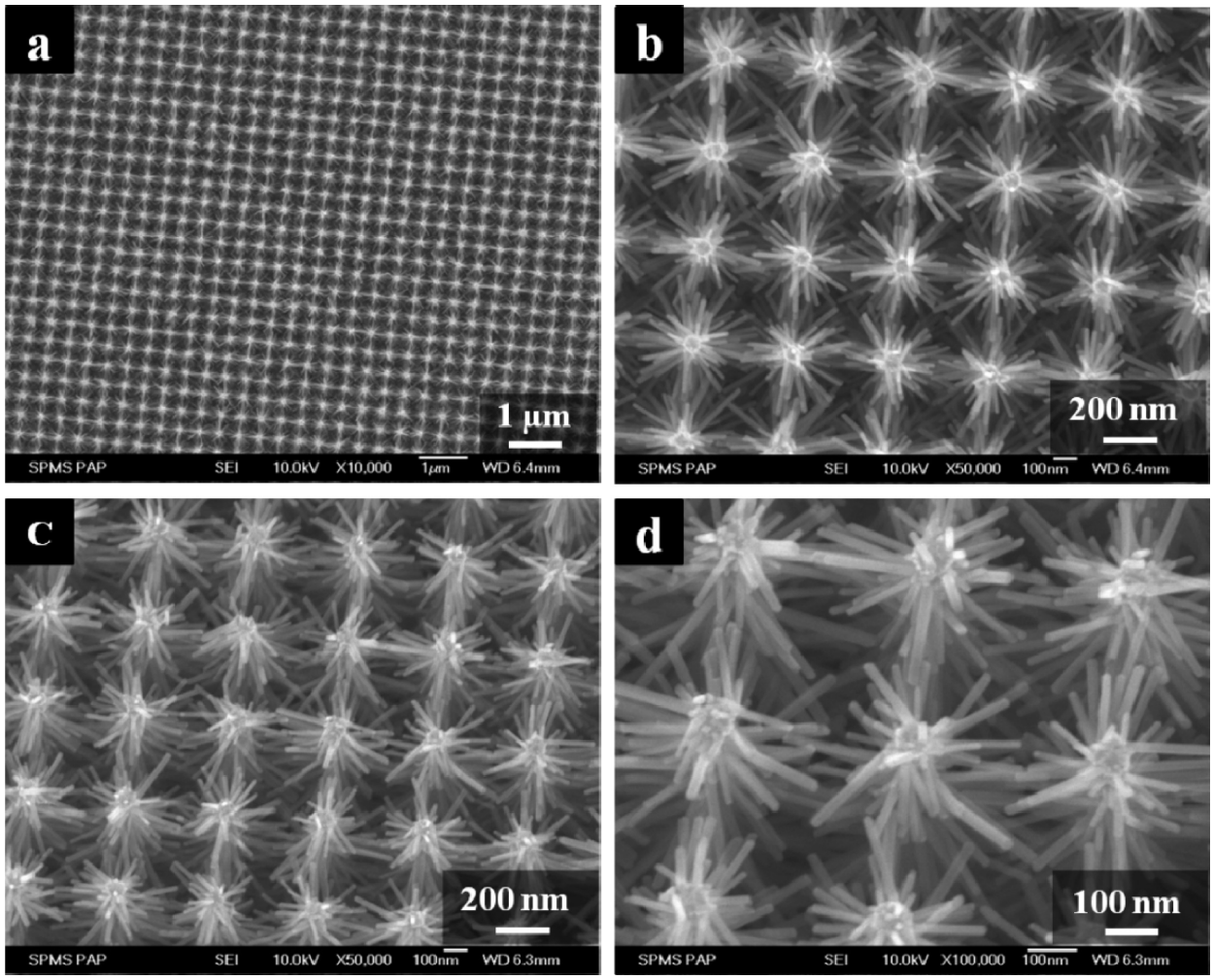

FIGURE 3. SEM images of the ordered Si/ZnO nanotrees. (a, b) Top view and (c, d) 20° titled view.

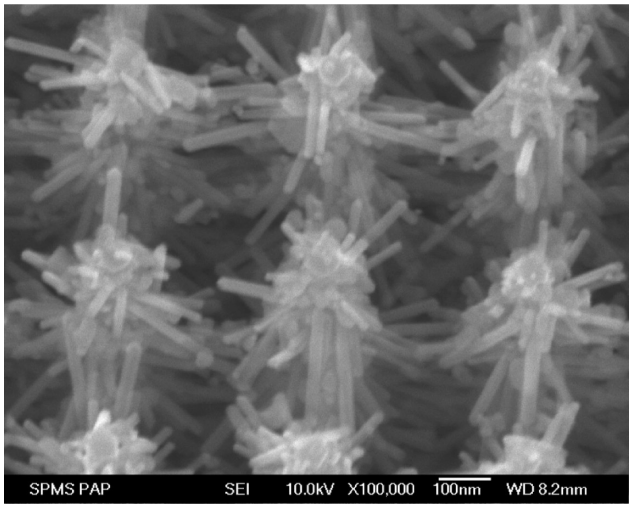

FIGURE 4. SEM image of Ag-nanoparticle-decorated Si/ZnO nanotrees used for the SERS measurement.

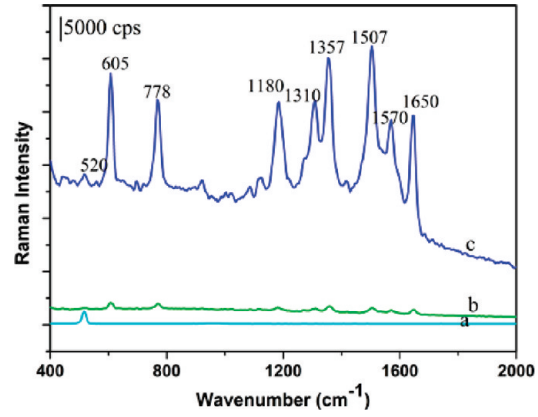

FIGURE 5. SERS spectra of R6G molecule with a concentration of 1 × 10^{-5} M collected from (a) Si/ZnO nanotrees; (b) 2D Ag nanoparticles substrate prepared by sputtering method; (c) Ag-nanoparticle-decorated Si/ZnO nanotrees. Laser wavelength, 532 nm; excitation power, 20 μW; data acquisition time, 0.5 s.

(or otherwise plausible assumptions) of the area density of the adsorbed molecules. We make a rough estimation of EF by using a reference sample (10^{-2} M R6G on quartz substrate) without SERS effect based on the formula $EF=(I_{1507,SERS}/I_{1507,ref})/(C_{SERS}/C_{ref})$, where $I_{1507,SERS}$ and $I_{1507,ref}$ denote the integrated intensities for the 1507 cm^{-1} band of R6G molecules, respectively. C_{SERS} and C_{ref} are the concentrations of the R6G molecules in the SERS and referece samples. In our work, the EF is estimated to be about 1 × 10^6.

The large SERS enhancement in Ag-decorated Si/ZnO nanotree substrates can be primarily ascribed to the local strong electromagnetic effect, which is associated with the sharp edge of Ag particles and/or resonance coupling be-

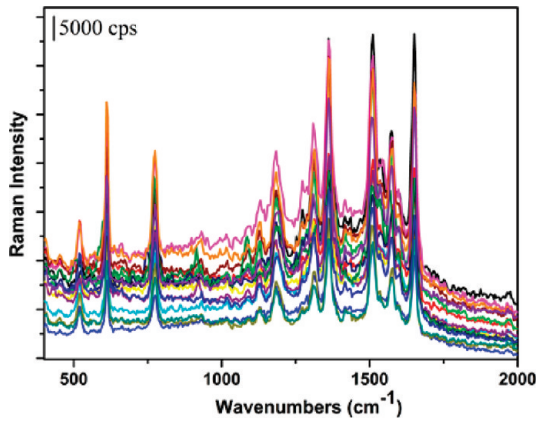

FIGURE 6. SERS spectra of R6G molecule with concentration of 1 × 10^{-5} M collected on the random-selected 15 places of the Ag-decorated Si/ZnO nanotrees. Laser wavelength, 532 nm; excitation power, 20 μW; data acquisition time, 0.5 s.

tween the adjacent Ag nanoparticles anchored on the ZnO surface (39, 40). The close interdistance between the Ag particles between the branches allows the formation of "hot spots", as a result, high SERS enhancement was obtained. To further clarify this issue, SERS measurement on Au nanoparticle-decorated Si/ZnO nanotrees was also conducted (see the Supporting Information, Figure S6 and7). The observed Raman signal is much weaker compared with that of Ag decorated Si/ZnO. This can be ascribed to the absence of strong electromagnetic field effect in Au nanoparticles under a 532 nm laser excitation. In addition, the periodic ordered 3D nanostructures might also enhance the excitation light trapping in Si/ZnO structures (41), consequently increasing the light interaction with Ag nanoparticles. This may also have contributed to the SERS enhancement.

The 3D Si/ZnO hierarchial structures with high-density ZnO branches provide a much larger surface area for loading Ag nanopartilces in comparison with that of 2D planar substrates. One may argue that the Raman ehnacement is actually due to a geometry effect, that is, the increased adsorption of R6G molecules in the nanotrees compared with 2D surfaces causes stronger Raman signal in the given excitation area. We claim that although this goemtry effect can give a small contribution to the enhancement, it is not the dominating reason. As mentioned above and shown in Figure S7 in the Supporting Information, the Au-decorated nanotrees give only weak Raman signal, which indicates that the enhancenment observed in Figures 5−6 is exclusively related with Ag nanoparticles and the 3D structure.

For practical SERS applications, signal reproducibility is one of essential parameters. To test the signal reproducibility of our sample, SERS spectra of R6G molecules with a concentration of 1 × 10^{-5} M from 15 randomly selected places on the Si/ZnO/Ag substrate were collected under indentical experimental conditions. As shown in Figure 6, the Raman spectra of R6G are enhanced greatly at each acquisition points, indicative of good SERS activity and reproducibility of the Si/ZnO/Ag hierarchical structures. However, there are still slight fluctuations in the peak intensities, which may be due to the nonuniform adsorption of Ag nanoparticles and/or R6G molecules.

CONCLUSION

We have presented a facile and new strategy for the creation of SERS-active substrates based on wafer-scale 3D ordered arrays of Si/ZnO nanotrees decorated with Ag nanoparticles. The SERS substrates exhibit excellent performance in terms of high sensitivity and good reproducibility. By comparing to Ag-deposited 2D substrates adn Au-coated nanotrees, the Raman enhancement is ascribe primarily to the electromagnetic field enhancement by the Ag nanoparticles, with a possible small contribution from the enhanced light trapping due to multiscattering.

The reason we demonstrate the ZnO-Si heterostructures herein is because of the easy growth of ZnO nanorods on various types of backbones. Nevertheless, such nano hierarchial SERS substrate is by no means limited to ZnO nor Si; instead it can be constructed based on other material combinations such as ZnO-SnO_2 (4), ZnO-carbon nanotube arrays (42). Such ordered Si/ZnO/Ag structures may be further integrated on a lab-on-chip device for label-free chemical and biomolecules detection processes.

EXPERIMENTAL METHOD

Fabrication of Si/ZnO Nanotrees. The fabrication process for the ordered array of Si/ZnO nanotrees is illustrated as in Figure 1. First, Si nanopillar arrays were prepared by a top-down photolithography patterning and followed by dry etching with ICP-RIE system and wet etching for metal/oxide removal. Second, ZnO nanorod branch structures were grown on Si nanopillars by a hydrothermal process adopted by our previous publication (4). Before the solution growth, the Si nanopillars were coated with a ~10 nm thick ZnO layer by atomic layer deposition (ALD). The ALD was performed with a Beneq TFS-200 system using diethyl zinc (DEZ) and DI water as Zn and oxygen precursors, respectively. The ZnO was grown at 200 °C using reactant exposure times of 500 ms for DEZ and H_2O, with 10 s nitrogen purge times between exposures. Subsequently, by putting the Si nanopillars array substrate into 35 mL aqueous solution of 0.025 M zinc nitrate [$Zn(NO_3)_2 \cdot 6H_2O$] and hexmethylenetetramine ($C_6H_{12}N_4$), the hydrothermal process was conducted at 95 °C for 3 h. After reaction, the substrates were removed from the solution, rinsed with deionized water, and dried by a N_2 flow.

Metal Nanoparticle Decoration and SERS Substrates Preparation. Ag nanoparticles were deposited on the Si/ZnO hierarchical structures by a photochemical deposition method. The as prepared Si/ZnO structures were immersed into 0.1 M $AgNO_3$ (equal volum water and ethanol) solution for 20 min to reach the Ag^+ adsorption equilibrium on the ZnO surface. Then the systems were irradiated under a 25 W UV lamp with a maximum emission at 365 nm for 3 min. After irradiation, the samples were carefully washed with deionized water and then dried by N_2 flow. Rhodamine 6G (R6G) was selected as the probe molecule for SERS measument. Fresh R6G solution with 1 × 10^{-5} M contrentration was prepared, then the samples were submerged in the R6G solution for 20 min, taken out, and washed thoroughly by deionized water.

Characterizations. The morphology and the crystalline structure of the as fabricated Si/ZnO and Si/ZnO/Ag hierarchical structures were characterized by JEOL JSM-6700F field emission scanning electron microscope (FE-SEM) and Bruker D8 Advanced X-ray powder diffraction (XRD) diffractometer with Cu Kα radiation. Raman measurements were performed at room temperature on a WITEC CRM200 Raman system with a 532 nm line laser as excitation. The laser spot area was ~1 μm in diameter and the incident power was 20 μW. It should be noted

that the accumulation times and the laser power are the same for all the Raman spectra.

Supporting Information Available: SEM images of Si/ZnO nanotrees with different ZnO nanorod lengths, Ag-nanoparticle-decorated nanotrees, Au-decorated Si/ZnO nanotrees, and Ag nanoparticles on flat Si substrate, additional SERS spectra, XRD patterns (PDF). This material is available free of charge via the Internet at http://pubs.acs.org

REFERENCES AND NOTES

(1) Qian, F.; Li, Y.; Gradecak, S.; Park, H.-G.; Dong, Y. J.; Ding, Y.; Wang, Z. L.; Lieber, C. M. *Nat. Mater.* **2008**, *7*, 701–706.
(2) Mieszawska, A. J.; Jalilian, R.; Sumanasekera, G. U.; Zamborini, F. P. *Small* **2007**, *3*, 722–756.
(3) Matthew, J. B.; Song, J *Energy Environ. Sci.* **2009**, *2*, 1050–1059.
(4) Cheng, C. W.; Liu, B.; Yang, H. Y.; Zhou, W. W.; Sun, L; Chen, R.; Yu, S. F.; Zhang, J. X.; Gong, H.; Sun, H. D.; Fan, H. J. *ACS Nano* **2009**, *3*, 3069–3076.
(5) Banholzer, M. J.; Millstone, J. E.; Qin, L. D.; Mirkin, C. A. *Chem. Soc. Rev.* **2008**, *37*, 885–897.
(6) Yang, R.; Chueh, Y. L.; Morber, J. R.; Snyder, R.; Chou, L. J.; Wang, Z. L. *Nano Lett.* **2008**, *7*, 269–275.
(7) Matthew, J. B.; Albert, L. Y.; Alexander, K. V. K.; Andrew, L. S.; Song, J. *Science* **2008**, *20*, 1060–1063.
(8) Dick, K. A.; Deppert, K.; Larsson, M. W.; Martensson, T.; Seifert, W.; Wallenberg, L. R.; Samuelson, L. *Nat. Mater.* **2004**, *3*, 380–384.
(9) Yang, X. F.; Zhuang, J. L.; Li, X. Y.; Chen, D. H.; Ouyang, G. F.; Mao, Z. Q.; Han, Y. X.; He, Z. H.; Wu, M. M.; Yu, J. C. *ACS Nano* **2009**, *3*, 1212–1218.
(10) Fleischman, M.; Hendra, P. J.; Mcquillan, A. J. *Chem. Phys. Lett.* **1974**, *26*, 163–166.
(11) Jeanmaire, D. L.; Van Duyne, R. P. *J. Elecroanal. Chem.* **1977**, *84*, 1–20.
(12) Albrecht, M. G.; Creighton, J. A. *J. Am. Chem. Soc.* **1977**, *99*, 5215–5217.
(13) Nie, S. M.; Emory, S. R. *Science* **1997**, *275*, 1102–1106.
(14) Ko, H.; Singamaneni, S.; Tsukruk, V. V. *Small* **2008**, *4*, 1576–1599.
(15) Doering, W. E.; Piotti, M. E.; Natan, M. J.; Freeman, R. G. *Adv. Mater.* **2007**, *19*, 3100–3108.
(16) Qin, L.; Zhou, S.; Xue, C.; Atkinson, A.; Schatz, G. C.; Mirkin, C. A. *Proc. Natl. Acad. Sci.* **2006**, *103*, 13300–13303.
(17) Gunawidjaja, R.; Peleshanko, S.; Ko, H.; Tsukruk, V. V. *Adv. Mater.* **2008**, *20*, 1544–1549.
(18) Qian, X.; Peng, X. H.; Ansari, D. O.; Yin-Geon, Q.; Chen, G. Z.; Shi, D. M.; Yang, L.; Yong, A. N.; Wang, M. D.; Nie, S. M. *Nat. Biotechnol.* **2008**, *26*, 83–90.
(19) Baker, G. A.; Moore, D. S. *Anal. Bioanal. Chem.* **2005**, *382*, 1751.
(20) Sun, Y. G.; Wiedrrecht, G. P. *Small* **2007**, *3*, 1964–1975.
(21) He, D.; Hu, B.; Yao, Q. F.; Wang, K.; Yu, S. H. *ACS Nano* **2009**, *3*, 3993–4002.
(22) Kim, J. H.; Kang, T.; Yoo, S. M.; Lee, S. Y.; Kim, B.; Choi, Y. K. *Nanotechnology* **2009**, *20*, 235302–235307.
(23) Yang, M. X.; Chen, T.; Lau, W. S.; Wang, Y. Q.; Tang, H.; Yang, Y. H.; Chen, H. Y. *Small* **2009**, *5*, 198–202.
(24) Chan, S.; Kwon, S.; Koo, T.; Lee, L.; Berlin, A. A. *Adv. Mater.* **2003**, *15*, 1595–1598.
(25) Ko, H.; Tsukruk, V. V. *Small* **2008**, *4*, 1980–1984.
(26) Chattopadhyay, S.; Lo, H. C.; Hsu, C. H.; Chen, L. C.; Chen., C. H. *Chem. Mater.* **2005**, *17*, 553–559.
(27) Zhang, B. H.; Wang, H. S.; Lu, L. H.; Ai, K. L.; Zhang, G.; Cheng, X. L. *Adv. Funct. Mater.* **2008**, *18*, 2348–2355.
(28) Deng, S; Fan, H. M.; Zhang, X.; Loh, K. P.; Cheng, C. L.; Sow, C. H.; Foo, Y. L. *Nanotechnology* **2009**, *20*, 175705–175710.
(29) Chen, L. M.; Luo, L. B.; Chen, Z. H.; Zheng, M. L.; Zapien, J. A.; Lee, C. S.; Lee, S. T. *J. Phys. Chem. C* **2010**, *114*, 93–100.
(30) Chen, J. N.; Mårtensson, T.; Dick, K. A.; Deppert, K.; Xu, H. Q.; Samuelson, L.; Xu, H. X. *Nanotechnology* **2008**, *19*, 275712–275716.
(31) Knoll, A. *Annu. Rev. Phys. Chem.* **1998**, *49*, 569–638.
(32) Abu Hatab, N. A.; Oran, J. M.; Sepaniak, M. J. *ACS Nano* **2008**, *2*, 377–385.
(33) Bhuvana, T.; Kulkarni, G. U. *Small* **2008**, *4*, 670–676.
(34) Tan, R. Z.; Agarwal, A.; Balasubramanian, N.; Kwong, D. L.; Jiang, Y.; Widjaja, E.; Garland, M. *Sens. Actuators, A* **2007**, *139*, 36–41.
(35) Hulteen, J. C.; Van Duyne, R. P. *J. Vac. Sci. Technol., A* **1995**, *13*, 1553–1558.
(36) Hulteen, J. C.; Treichel, D. A.; Smith, M. T.; Duval, M. L.; Jensen, T. R.; Van Duyne, R. P. *J. Phys. Chem. B* **1999**, *103*, 3854–3863.
(37) Wang, Y.; Wang, M. L.; Liu, J. Q.; Scholz, R.; Peng, J.; Christiansen, S.; Kim, D. H.; Steinhart, M. *Nano Lett.* **2009**, *9*, 2384–2389.
(38) Hildebrandt, P.; Stockburger, M. *J. Phys. Chem.* **1984**, *88*, 5935–5944.
(39) Garcia-Vidal, F. J.; Pendry, J. B. *Phys. Rev. Lett.* **1996**, *77*, 1163–1165.
(40) Wang, H. H.; Liu, C. Y.; Wu, S. B.; Liu, N. W.; Peng, C. Y.; Chan, T. H.; Hsu, C. F.; Wang, J. K.; Wang, Y. L. *Adv. Mater.* **2006**, *18*, 491–495.
(41) Pai, Y. H.; Meng, F. S.; Lin, C. J.; Kuo, H. C.; Hsu, S. H.; Chang, Y. C.; Lin, G. R. *Nanotechnology* **2009**, *20*, 035303—035309.
(42) Zhang, W. D. *Nanotechnology* **2006**, *17*, 1036–1040.

AM100270B